Soluble TREM2 induces microglia dysfunction and brain damage while cleavage-reduced TREM2 shows sustained microglia activation with enhanced remyelination in the cuprizone model

Nicolau Beckmann
Novartis Institutes for BioMedical Research Basel
Anna Neuhaus
Novartis Institutes for BioMedical Research Basel
Stefan Zurbruegg
Novartis Institutes for BioMedical Research Basel
Stefanie Joller
Novartis Institutes for BioMedical Research Basel
Dominik Feuerbach
Novartis Institutes for BioMedical Research Basel
Arno Doelemeyer
Novartis Institutes for BioMedical Research Basel
Tatjana Schweizer
Novartis Institutes for BioMedical Research Basel
Stefan Rudin
Novartis Institutes for BioMedical Research Basel
Ulf Neumann
Novartis Institutes for BioMedical Research Basel
Ramon Berth
Novartis Institutes for BioMedical Research Basel
Wilfried Frieauff
Novartis Institutes for BioMedical Research Basel
Fabrizio Gasparini
Novartis Institutes for BioMedical Research Basel
Derya R. Shimshek (derya.shimshek@novartis.com)
Novartis Pharma AG https://orcid.org/0000-0001-8602-7850

Research article

Keywords: TREM2, microglia, neuroinflammation, cuprizone, MRI

Posted Date: March 25th, 2022

DOI: https://doi.org/10.21203/rs.3.rs-1431273/v1

Abstract

Triggering receptor expressed on myeloid cells 2 (TREM2) is a cell-surface immunoreceptor expressed on microglia, osteoclasts and monocytes/macrophages. In humans, homozygous loss-of-function mutation carriers exhibit bone cysts and fractures with an early-onset frontal lobe syndrome and progressive presenile dementia known as Nasu-Hakola. Neuropathological findings include myelin/neuronal loss and neuroinflammation. Heterozygous loss-of-function mutation in TREM2 has been associated with several neurodegenerative diseases like Alzheimer`s disease and Frontotemporal Dementia. We investigated the involvement of soluble and cleavage-reduced TREM2 on central myelination processes by using different gene-modified animals expressing (cleavage-reduced (TREM2-IPD), soluble-only (TREM2-sol), knock-out (TREM2-KO) TREM2and wildtype (WT) mice in the cuprizone model.. In the acute cuprizone model all genotypes showed demyelination detected by T2-weighted signal intensity increase in Magnetic resonance imaging (MRI), most prominent in the external capsule (EC) and less in the corpus callosum. In the 4-week recovery phase a partial signal reduction in WT and TREM2-IPD was observed, while in TREM2-sol and TREM2-KO showed an increase in MRI signal in the EC. In TREM2-IPD histology revealed no recovery of neuroinflammation as well as of the lysosomal marker LAMP-1, which was also evidenced in enhanced cytokine/chemokine levels. This persistent microgliosis and astrocytosis was also observed in TREM2-sol, to a lesser extent in TREM2-KO during recovery with both homeostatic (TMEM119) as well as activated (LAMP-1) microglia markers increased. An increase in cytokines/chemokines was not evident. This was accompanied, specifically in the EC with no myelin recovery, appearance of myelin debris and axonal pathology, while oligodendrocytes recovered. In the chronic cuprizone model TREM2-IPD displayed sustained microgliosis and enhanced remyelination in the recovery phase. Taken together, our data suggest that sustained microglia activation leads to increased remyelination, whereas microglia without membrane-functional or complete loss of TREM2 results in a dysfunctional phenotype with improper myelin debris removal, lack of remyelination and axonal pathology.

Background

Triggering-receptor expressed on myeloid cells 2 (TREM2) is a cell-surface immunoreceptor expressed on microglia, dendritic cells, osteoclasts and other tissue-resident macrophages [19]. In humans, TREM2 homozygous loss-of-function mutation carriers exhibit bone cysts and fractures during adolescence, together with an early-onset frontal lobe syndrome and progressive presenile dementia known as Nasu-Hakola [6, 51]. Neuropathological findings include myelin and neuronal loss as well as increased neuroinflammation. Furthermore, strong genetic links of TREM2 mutations to Alzheimer $sdisease(AD), Fron \rightarrow temp$ or $alDementia(FTD), Park \in son$s disease (PD) and Amyotrophic Lateral Sclerosis (ALS) have been found [19]. It is hypothesized that TREM2 expression increases at the peak of disease and drives its resolution, by acting as a phagocytosis receptor, supporting microglia survival/migration and modulating cytokine release. In different disease contexts it has been observed that absence of functional TREM2 seems to lock microglia in a homeostatic and/or not fully activated phenotype and thus, to slow down autophagy and hamper resolution of inflammation [20, 32, 39, 47, 50].

On the other side, it has been shown that antibodies that enhance TREM2 activity lead to a protective effect of microglia [42, 49]. Furthermore, cleavage-reduced TREM2 mice in the context of Aβ pathology show an acceleration of microglia response [7].

The cuprizone-induced demyelination model enables to study different myelination and neuroinflammation stages in the central nervous system [12, 21, 41, 43, 46, 53]. It has been shown previously that TREM2 knockout (TREM2-KO) mice displayed altered microglia responses to cuprizone intoxication as well as reduced clearance of myelin debris [3, 37]. Furthermore, it has been shown that TREM2 is essential for remyelination processes in the lysolecithin model [11] and TREM2 is important in cleaning up toxic lipids in multiple sclerosis [8].

Here, we investigated the involvement of sustained TREM2 activation and soluble TREM2 on myelination and neuroinflammation processes in the cuprizone model by using gene-modified animals and applying magnetic resonance imaging (MRI) and histology [2, 44].We show for the first time that sustained TREM2 activation in the cleavage-reduced TREM2-IPD mouse increases microglia activation and enhances remyelination in the recovery phase, while soluble-only TREM2 (TREM2-sol) leads to dysfunctional microglia with distinct differences to microglia lacking TREM2 (TREM2-KO, in particular massive increase in the lysosomal marker LAMP-1. On the other hand, TREM2-sol and TREM2-KO both lead to enhanced myelin debris, axonal pathology, and absence of remyelination in the recovery phase.

Material And Methods

Statement on animal welfare

In vivo experimental procedures followed the Swiss animal welfare regulations. Studies described in this report were approved by the Swiss Cantonal Veterinary Authority of Basel City, Switzerland, and performed under the license number BS-2711. Authors complied with the ARRIVE guidelines for animal experimentation.

Animals

TREM2-KO mice [18] were purchased from the UC Davis KOMP Repository (Project ID VG10093) and were then bred at Novartis Pharma AG (Basel, Switzerland) in the C57BL/6 background. Wildtype (WT) mice were either littermates from a TREM2 heterozygous KO breeding or C57BL/6J from Charles River (Sulzfeld, Germany). TREM2-IPD mice were generated as described earlier [7]. The TREM2-sol (TREM2 soluble-only, B6-Trem2em3Npa) knock-in (KI) mice were generated at the Novartis Institutes for BioMedical Research (NIBR, Cambridge, USA). In brief, two single guide RNAs (sgRNAs) and a donor oligo (200 bp) containing the stop-codon TGA after the amino acid H and including a restricting enzyme site Eco57I (CACTGAAGC) replacing the wildtype amino-acids HST (CACAGCACC) were designed to target the mouse TREM2 allele. The sgRNAs (sgRNA1, complementary sequence: 5’-gggaccactactgtacct; sgRNA2, forward sequence: 5’- aagtggaacacagcacctcc) were ordered as crisp RNAs (crRNAs) from Integrated DNA Technologies (IDT, Coralville, IA, USA) as part of their Alt-R CRISPR/Cas9 system. sgRNA1 or sgRNA2 was

microinjected, along with the universal Alt-R tracrRNA (IDT, IA, USA), donor oligo and Cas9 protein (PNA Bio, Thousand Oaks, CA, USA), into the pro-nucleus of fertilized C57Bl/6J oocytes. Viable two-cell embryos were re-implanted in pseudo-pregnant B6CBAF1 females. The resulting pups were genotyped by PCR analysis (primer F1: 5-$agctacgctactgcaaag,'rR1:5$-cccgatgagctcttccacat, expected product length: 635 bp, PCR program: 95°C 3 min, 95°C 20 sec, 60°C 20 sec, 72°C 45 sec, go to step 2, 35 cycles, 72°C 5 min, 14°C forever), followed by XhoI digestion and Sanger sequencing. Eight KI founders were back-crossed with C57BL/6J mice (JAX stock #000664, The Jackson Laboratory, Bar Harbor, ME, USA) and the F0 and F1 generation was subjected to MiSeq sequencing (Illumina Inc, San Diego, CA, USA) using a forward primer 5-$atgctggagatctctgg>$ and $areverse'r5$-gtgagttgctacaaagggctcc to generate amplicons, and NuGEN's Amplicon Sequencing System (part number 9092 – 256, Tecan, Redwood City, CA, USA) for the construction of a Next-Generation Sequencing library. Two founder lines were chosen. One mouse of each founder line (heterozygous) was subjected to targeted locus amplification (TLA) at Cergentis (Utrecht, The Netherlands). For this, viable frozen mouse spleen cells were used and processed according to Cergentis' TLA protocol [48]. Two primer sets were designed on the transgene (Set 1: reverse primer exon 3: 5-$GGTCATCTAGAGGGTCTGTA,for ward'rexon3:5$-TTCGTGCACTTAGTAGATCC; Set 2: reverse primer HA: 5-$CTACTGGGTTGTCATG,for ward'rHA:5$- GAACGTTAGCCTGTCTCTAG). The primer sets were used in individual TLA amplifications. PCR products were purified and library prepared using the Illumina Nextera flex protocol and sequenced on an Illumina sequencer. Reads were mapped using the Burrows-Wheeler Aligner's Smith-Waterman (BWA-SW) alignment algorithm [26], version 0.7.15-r1140, settings bwasw -b 7. The NGS reads were aligned to the transgene sequence and the host genome. The mouse mm10 genome was used as host reference genome sequence. The presence of single-nucleotide variants (SNVs) was determined using samtools mpileup (samtools version 1.3.1, Genome Research Limited, Hinxton, UK) [25, 27]. Fusion sequences consisting of two parts of the transgene were identified using a proprietary Cergentis script. Fusions resulting from the TLA procedure itself were recognized by the restriction enzyme-specific sequence at the junction site and removed. Integration sites were detected based on a) coverage peak(s) in the genome and b) the identification of fusion-reads between the transgene sequence and the host genome. The transgene of both samples were integrated in mouse chr17:48,351,169 – 48,351,193 as intended. Genotyping has been performed from ear punch or tail tip DNA by two different PCRs with GotTaq (Promega, Madison, WI, USA) with the following primers: (i) PCR with Knock-in with primer sets 996_sTrem2-KI_F (5-$gatagggaatcgaagaggc$) and 997_sTrem2 - KI_R(5-ctactgtacctactcgtgcttcag) as well as internal control for beta-actin (747-beta-actin-fw-1: 5-TGTGGGCATTTGATGAGCCGG; 748-beta-actin-rev-1: 5-AAGACCCAGAGGCCATTGAGG); (ii) PCR with wildtype primer sets 994_sTrem2-wt_F (5-tggaacacagcacctccagg) and 995_sTrem2-wt_R (5- gggcttcatgtggctcaggg) as well as internal control for beta-actin with primer pair (747-beta-actin-fw-1 and. 748-beta-actin-rev-1. Expected KI band size: 251 bp, wildtype band size: 468 bp. Internal beta-actin control: 122 bp. PCR program: 95°C 3 min, 95°C 30 s, 60°C 30 s, 72°C 30 s, go to step 2, 35 cycles, 72°C 5 min, 8°C forever.

All animals were female, 2–3 months old at the beginning of the study, and divided into n = 4–7 mice per group.Genotyping of TREM2-KO mice was performed according to the protocol by UC Davis KOMP. All animals were allowed to adapt for 7 days prior to the start of the experiment and housed in individual ventilated cages (max. 4 mice/XJ Type cage). Mice were given access to food and water ad libitum throughout the study.

Cuprizone treatment

Animals were treated with cuprizone for 5 (acute model) or 12 (chronic model) weeks and then switched to normal food for 3 or 4 weeks. Cuprizone [Bis(cyclohexanone) oxaldihydrazone, Sigma-Aldrich, Buchs, Switzerland] was mixed into rodent food pellets (0.2% w/w) by Granovit AG (Kaiseraugst, Switzerland). Three independent studies for the acute model were performed. 1. Study: TREM2-KO (hom), TREM2-KO (het) and WT; 2. Study: TREM2-IPD, TREM2-sol (hom) and WT; 3. Study: TREM2-sol (het) and WT.

Magnetic resonance imaging (MRI)

Measurements were performed with a Biospec 70/30 spectrometer (Bruker Medical Systems, Ettlingen, Germany) operating at 7 T. The operational software of the scanner was Paravision 5.1 (Bruker). Images were acquired from anesthetized, spontaneously breathing animals using a mouse brain circularly polarized coil (Bruker, Model 1P T20063V3; internal diameter 23 mm) for radiofrequency excitation and detection. Neither cardiac nor respiratory triggering was applied. Following a short period of introduction in a box, animals were maintained in anesthesia with 1.5% isoflurane (Abbott, Cham, Switzerland) in oxygen, administered via a nose cone. During MRI signal acquisitions, animals were placed in prone position in a cradle made of Plexiglas, the body temperature was kept at 37 ± 1°C using a heating pad, and the respiration was monitored.

A T_2-weighted, two-dimensional multislice RARE (Rapid Acquisition with Relaxation Enhancement) sequence [16] was used for selecting the regions-of-interest (ROIs) and for evaluating signal intensities. A two-dimensional multislice gradient-recalled FLASH (Fast Low-Angle Shot) acquisition [13] served to assess the magnetization transfer ratio (MTR), a measure reflecting myelin content (Beckmann et al., 2018). Assessments of the relaxation time T_2 were performed using a multislice spin-echo sequence. As the three sequences had the same anatomical parameters, the ROIs for evaluations were selected on the RARE images and then transferred to the FLASH and spin-echo images. MRI images were analyzed using the Paravision software.

The parameters of the acquisitions were the following: (a) RARE sequence: effective echo time (TE) 80 ms, repetition time (TR) 3280 ms, RARE factor 16, 12 averages. Hermite pulses of duration/bandwidth 1 ms/5400 Hz and 0.64 ms/5344 Hz were used for radiofrequency excitation and refocusing, respectively. Fat suppression was achieved by a gauss512 pulse of 2.61 ms/1051 Hz duration/bandwidth followed by a 2-ms-long gradient spoiler. The total acquisition time was of 7 min 52.3 s; (b) FLASH sequence: TE/TR 2.8/252.8 ms, 4 averages. A hermite pulse of 0.9 ms/6000 Hz duration/bandwidth and flipangle 30° was used for radiofrequency excitation. MTR contrast was introduced by a gauss pulse of 15 ms/182.7 Hz

duration/bandwidth applied with radiofrequency peak amplitude of 7.5 µT and an irradiation offset of 2500 Hz. The acquisition was then repeated with the same parameters but without the introduction of the MTR contrast. MTR was then computed using the formula MTR=(S_0-S_{MTR})/S_0, where S_0 and S_{MTR} represent respectively the signal intensities in the FLASH acquisitions without and with the introduction of the MTR contrast. The total acquisition time for both data sets was of 6 min 31.6 s; (c) Finally, assessments of the relaxation time T_2 were performed using a multislice spin-echo sequence with the parameters: 16 echoes spaced by 11 ms, TE from 11 to 176 ms, TR 3000 ms, fat suppression as described above. T_2 was determined by exponentially fitting with Origin2021 (OriginLab, Northampton, MA, USA) the mean signals as function of TE from ROIs placed in the corpus callosum (cc) and the external capsule (ec). All three sequences were run using the same anatomical parameters: field-of view 20x18 mm^2, matrix size 213x192, pixel size 0.094x0.094 mm^2, slice thickness 0.5 mm, 15 adjacent slices.

Post-mortem **analyses**

Before animals were perfused trans-cardiacally by phosphate-buffered saline under isoflurane anesthesia, blood was withdrawn by heart-puncture. Brains were removed from the skull and the forebrain (excluding olfactory bulb, brainstem and cerebellum) was used for biochemical assessments and histology. In the study with the TREM2-KO animals were also perfused with 4% paraformaldehyde. All brains subjected for histology were fixed in 4% paraformaldehyde for 48 h at 4°C. Analyses were performed blind to the genotype and treatment of the mice.

Mouse TREM2 determination from brain and cell culture supernatant

Mouse forebrain was homogenized in 1:10 (w/v) Tris-buffered saline (TBS) containing Complete protease inhibitor (Roche Diagnostics, Switzerland) using an ultrasonic device. Fifty microliters of TBS containing Complete Protease inhibitor were mixed with 50 µl of homogenate and incubated on ice, with regular vortexing for 15 minutes. The extract was centrifuged for 15 minutes at 100000xg and the clear supernatant (50 µl) was transferred to the ELISA plate. Medium from cultures of bone marrow derived macrophages (BMDM) was collected, spun down at 1000 RPM for 5 minutes and 25 µl of the supernatant was added onto the coated 96-well plates. Polyclonal sheep anti-TREM2 antibody AF1729 (R&D Systems, Minneapolis, MN, USA) at 0.2 mg/ml in PBS was used as coating antibody. Samples were incubated for two hours and the plate was washed. For detection, wells were filled with 50 µl of 0.5 µg/ml of biotinylated anti-TREM2 antibody AF1729 (R&D Systems), incubated 1 hour at room temperature and washed. Streptavidine-horseradish peroxidase (# 893975, R&D Systems) and tetramethylbenzidine/H_2O_2 substrate were added

at room temperature, and the reaction was stopped after 20 minutes by addition of 2 N sulfuric acid. Absorbance at 450 nm was read with a SpectraMax Plus 384 reader (Molecular Devices, San Jose, CA, USA). Recombinant mouse TREM2 (Novoprotein, Wuijang, PR of China, Cat # CM92) from 39 pg/ml to 2500 pg/ml was used as standard.

Cytokine/chemokine measurements

Half brains were dounce homogenized 1:10 (w:v) in TBS, aliquoted and stored at -80°C. Radioimmunoprecipitation assay buffer (Merck Millipore 20–188) was added ten times to an aliquot, mixed and incubated on ice for 10 min, then centrifuged for 5 min at 10000rcf at 4°C. Supernatants (1:2 in diluent 41) were used for U-plex (mouse) Meso Scale Discovery (Acro Biosystems, Newark, DE, USA) electrochemiluminescence analyses according to manufacturer`s protocol.

Mouse plasma NF-L measurements

Plates (MesoScale Discovery (MSD) Multi Array 96well, L15XA-3) were coated with 25µL capture antibody working solution 25µL/ well (Uman Diagnostics, α-NF-L mAb 47:3 (UD1); 2.35mg/ml; diluted in PBS to 0.5ug/mL), shaked for 10min and incubated overnight at 4^0C. Plates were washed 3x with 150µl wash buffer (0.05% Tween20 (Sigma, CAS 9005-64-5) in 1xTBS (Sigma, T5912-1L)). Blocking was performed with 150µL blocking buffer / well (2% BSA (fraction V) in wash buffer) and incubated 1h at room temperature. Plates were again washed 3x with 150µl wash buffer. Standard (NF-L, Uman Diagnostics, 27001) and plasma samples (dilution on plate 1:2 in 1xTBS with complete (protease inhibitor cocktail tablets (Roche)) were added (25µL per well, in sample dilution buffer (0.1% BSA in wash buffer)) and plates were sealed and incubated 2h at room temperature. Plates were washed 3x with 150µl wash buffer. Detection antibody (Uman Diagnostics, biotin labelled α-NF-L mAb 2:1 (UD3); 0.86 mg/ml; diluted to 0.5µg/ml in 0.5% BSA;) was added (25µL per well in detection antibody dilution buffer (0.5% BSA in wash buffer)) and plates were sealed and incubated for 1h at room temperature. Plates were washed 3x with 150µl wash buffer. Streptavidin SULFO TAG (MSD SulfoTag, CAT R32AD-1, 500µg/mL working dilution: 1:1000 in PBS) was added (25µL/well) and incubated for 30-60min at room temperature in the dark. Plates were washed 3x with 150µl wash buffer. 2xread buffer (Cat. R92TC-3, working solution 1:2 in destilled water) was added (150µL / well) and plates were analysed with the plate reader (MSD SECTOR Imager 600).

Culture of bone marrow-derived macrophages (BMDM)

BMDMs were prepared from three adult WT and TREM2-sol mice. Tibia and femur bones were dissected clean of surrounding muscle tissue and the marrow was flushed out using a 30G needle fitted onto a 10 ml syringe. The cell suspension was filtered through a 100 µm cell strainer and incubated for 5 minutes in red blood cell lysis buffer. Following centrifugation, BMDM were washed with PBS and resuspended in a RPMI1640 culture media containing 10% FBS (Gibco, 10082147), 1% Pen/Strep (Gibco, 15070063), 1% Sodium pyruvate (Gibco, 11360-070), 1% NEAA (Gibco, 11140035), 0.025 M HEPES (Gibco, 15630080), 50 µM β-Mercaptoethanol and 40 ng/ml M-CSF (R&D systems, 416-ML-050). Three days after seeding, cells were replenished with media containing 40 ng/ml M-CSF, 20 ng/ml M-IL4 (R&D systems, 404- ML-050) and 20 ng/ml M-IL13 (R&D systems, 413-ML-005). BMDM were used in experiments after one week of differentiation.

For measurement of cell surface TREM2 expression, BMDM were treated with either 5 μM DPC333 (Bristol-Myers Squibb, Princeton, NJ, USA) [10] O/N or with 50 ng/ml para-methoxyamphetamin (PMA, Sigma Aldrich, 19–144) for 30 minutes. Cells were detached using TrypLE enzyme (ThermoFisher, Basel, Switzerland, 12605010) once and incubated with FC block (anti-CD16/32; eBioscience, ThermoFisher, 14-0161-85) in FACS buffer (PBS containing 2% FBS, 0.5 mM EDTA and 0.05% sodium azide) for 20 minutes at 4°C. Then, cells were stained in suspension with biotinylated anti-mouse TREM2 antibody (R&D Systems, BAF1729) for 30 min at 4°C. Streptavidin-AF488 secondary antibody was added for 30 min at 4°C. Staining was analyzed in a Fluorescence Activated Cell Sorter (FACS) from BDBiosciences (FACSCanto) upon gating for LIVE/DEAD Fixable aqua (Molecular Probes, Eugene, OR, USA, L34966) to remove dead cells.

Phagocytosis by bone marrow-derived macrophages (BMDMs)

For in-vitro phagocytosis, BMDMs from WT and TREM2-sol mice were plated in Poly-L-lysine coated 96-well plates at seeding density of 40,000 cells/well and let attach for 3 hours. pHrodo™ Red LDL (ThermoFisher, L34356; 1 μg/ml) was diluted in BMDM medium and added to individual wells. The plates were placed in an IncuCyte S3 live cell analysis system (Agilent Technologies Switzerland, Basel, Switzerland) and four images per well were acquired every hour for 9 hours. The integrated fluorescence intensities were extracted for each well and analyzed in a GraphPad Prism software (Graphpad Software Inc., La Jolla, CA USA).

Histology of brains

After fixation, brains were processed for paraffin embedding by dehydration through increasing ethanol series. Paraffin sections of 3 μm thickness (coronal brain sections from the preoptic area, coordinates according to Paxino and Franklin: interaural 4.9–3.94 mm, Bregma 1.1–0.14 mm) mounted on SuperFrost + slides (Thermo Fisher Scientific, Reinach, Switzerland) were automatically immunostained using the Discovery XT technology (Ventana, Roche Diagnostics, Rotkreuz, Switzerland). Sections were deparaffinized, rehydrated, subjected to antigen retrieval by heating with CC1 cell conditioning buffer for 28–68 min according to the antibody, then incubated for 1–3 hours according to the primary antibody at room temperature with primary antibody diluted in antibody diluent (Ventana), incubated with the respective biotinylated secondary antibody diluted in antibody diluent, reacted with a DABMab kit (Ventana) and counterstained with Hematoxylin II and Bluing reagent (Ventana). Slides were washed with soap in hot tap water and rinsed under cold running tap water to remove the soap, then dehydrated and embedded with Pertex.

For luxol fast blue (LFB) staining, slides were deparaffinized and rehydrated to 95% ethanol. Slides were then incubated in LFB solution [Solvent Blue 38 (Sigma S3382) in 95% ethanol and 10% acetic acid (Sigma 695092)] overnight at 60°C, rinsed in 95% ethanol for 1 min, then in distilled water for 2 min and in 0.05% lithium carbonate (Merck 105680; Merck Millipore, Schaffhausen, Switzerland) for 5 s. Subsequently, slides were rinsed in 70% ethanol twice for 10 s, then in distilled water for 2 min. The

rinsing was repeated in 0.05% lithium carbonate prepared freshly, 70% ethanol and distilled water until there was a sharp contrast between the blue of the white matter (myelin) and the colorless grey-matter. Finally, slides were dehydrated starting with 95% ethanol and mounted in Pertex.

Antibodies

Primary antibodies were: rabbit anti-mouse myelin basic protein (MBP) (Dako A0623; Dako, Carpinteria, CA, USA) 1:1000; rabbit anti-mouse glutathione S-transferase-π (GST-π) (MBL 312; MBL International, Woburn, MA, USA) 1:500; Rabbit anti-Iba1 (Wako 019-19741, 50 µg/100 µl) 1:500; rabbit anti-GFAP (glial fibrillary acidic protein, Dako Z0334) 1:5000; rabbit anti-dMBP (debris of MBP) (Merck Millipore AB5864) 1:3000; mouse anti-Neurofilament (Covance SMI312; BioLegend Covance, San Diego, CA, USA) 1:5000; rat anti-LAMP-1 (CD107a, Bio-Rad, Cressier, Switzerland, MCA4707T) 1:200. Rabbit anti-TMEM119 (209064, abcam).

Secondary detection antibodies were: Goat anti-rabbit IgG biotinylated (Jackson ImmunoResearch 111-065-144; Jackson ImmunoResearch, Cambridgeshire, UK) 1:1000; Goat anti-rabbit IgG biotinylated (Vector BA-1000; Vector Laboratories, Peterborough, UK) 1:200 or 1:1000; Goat anti-mouse IgG biotinylated (Vector BA-9200) 1:1000

Analysis of histological images

For the quantitative evaluation of microglia numbers and morphology based on image analysis from histological stained coronal brain sections, a proprietary image analysis platform (ASTORIA, Automated Stored Image Analysis, Novartis Pharma AG, Basel, Switzerland) was developed based on MS Visual Studio 2010 (Microsoft, Seattle, WA, USA) and many functions from Matrox MIL V9 libraries (Matrox Inc., Dorval, Quebec, Canada) as described elsewhere [2]. One to two coronal brain sections (from the preoptic area, approximate coordinates according to Paxinos and Franklin: interaural 4.9–3.94 mm, Bregma 1.1–0.14 mm) per animal were used for image analysis at the level of the corpus callosum (cc) and the external capsule (ec).

The following procedure was followed for the detection and analysis of soma, proximal and distal processes as described earlier [2]: 1. Brain sections containing immunohistochemically stained microglia (Iba1) soma and their proximal and distal processes (all in brown) were scanned with Aperio's Scanscope (Leica Biosystems, Wetzlar, Germany) at 20x magnification. 2. Each image was processed using the ImageScope software (V12.1.0.5029, Aperio) according to the following steps: A: color deconvolution to obtain brown staining without blue; B: segmentation of brain tissue from white background through thresholding, morphological closing, filling of holes, opening and elimination of too small objects, resulting in a binary mask of the valid tissue and sample area; C: adaptive thresholding for the individual segmentation of soma, based on the average gray value of the blue channel of the color-deconvoluted brown image at sufficiently dark regions (indicative for soma). The computed threshold was used for binarization, and after size filtering yielded the soma mask image (within the valid sample region); D: segmentation of processes through morphological top hat transformation with a size to pick thin processes. Adaptive thresholding was applied again to segment the processes (using the previously

determined gray average of brown objects), followed by binarization of the top hat image and size filtering of the resulting objects; E: subtraction of soma (that may also have been picked by top hat thresholding) to obtain an image mask of true processes; F: ultimate thinning of processes for length computation; G: proximal processes: A predefined number of dilations of soma was used to define a reference (marker) region for proximal soma, employing a circle around the soma centre to define the cutoff boundary for proximal processes. Thinned proximal processes with marker in dilated soma and limited by circular influence zones (set of “proximal thinned processes”) were then reconstructed around the soma centre. “Final proximal processes” were collected through reconstruction of all processes having markers in the “proximal thinned processes” set; H: soma was added to proximal processes to obtain a set of “visible microglia”; I: Distal processes: Reconstruction of processes from proximal processes only (i.e. ignoring those in the background or from the soma in a different focus plane), then subtraction of circular regions defining proximal processes to yield a set of distal processes; J: in the optical density computation for soma as well as “visible microglia” (individual soma + proximal processes complex within circular reference region), local background (non-visible microglia) was used as reference; K: morphometric features (size, form factor, length) were computed for soma, proximal and distal processes.

This image analysis algorithm was also used to quantify stained area of oligodendrocytes (GST-π) and astrocytes (GFAP) stained coronal brain sections according to the above description. Luxol Fast Blue was analyzed by integrated optical density (IOD) parameter by ASTORIA.

HALO Image Analysis Platform (Indica Labs) was used to analyze myelin debris (dMBP), lysosomal marker (LAMP-1), neurofilament (SMI312) and homeostatic microglia marker (TMEM119).

Statistics

All data are presented as as means ± SEM. MRI data were analyzed using Anova with random effects (SYSTAT 13, SYSTAT Software, Inc.) to take the longitudinal character of the data into account. In vitro data was analyzed by mixed-effects analysis Sidak`s multiple comparison test or t-tests to compare two groups were performed as specified in the figure legends. To analyze histology data, either Holm-Sidak's one-way ANOVA tests with multiple test group effect per time point, Anova with random effects or t-tests to compare two groups were performed as specified in the figure legends. Statistical significance was assumed for $p < 0.05$.

Results

MRI and histology revealed similar demyelination in all genotypes but TREM2-sol and TREM2-KO mice showed accumulation of myelin debris, lack of remyelination and enhanced axonal pathology with partial oligodendrocyte recovery in the acute cuprizone model

Mice expressing TREM2 soluble-only were generated by introducing a stop-codon (TGA) into the cleavage-site of TREM2 [10] via CRISPR/CAS9 (see Material and methods for details, Fig. 1a). TREM2

expression was assessed in BMDMs, showing a complete absence of TREM2 from the cell surface (Fig. 1b), while in the supernatant soluble TREM2, albeit reduced, could be observed (Fig. S1a). Phagocytosis experiments in BMDMs from mice showed a reduced uptake of LDL-pHrodo in TREM2-sol compared to WT (Fig. 1C, Fig. S1b). This is similar to the impaired phagocytic activity observed in TREM2-KO [7].

Cleavage-reduced TREM2 (TREM2-IPD, IPD), soluble-only TREM2 only (TREM2-sol, sol, homozygous (hom) and heterozygous (het)), TREM2 knock-out (TREM2-KO, KO, homozygous (hom) and heterozygous (het)) and wildtype (TREM2-WT, WT) mice (Fig. 1a) were treated with 0.2% cuprizone in feed for 5 weeks and then switched to normal food (Fig. 1d). Noninvasive, longitudinal magnetic resonance imaging (MRI) was performed at the beginning (baseline), at 3 and 5 weeks during cuprizone intoxication and at 7 and 9 weeks during recovery on normal food (control food) (Fig. 1d, 1e). Analysis of T_2-weighted signal intensity for the CC and EC is summarized in Fig. 1F. MRI detected no difference between the different genotypes at baseline, i.e. at the beginning of the study before cuprizone intoxication (Fig. 1e, 1f). During cuprizone treatment, MRI signal in the CC and EC increased (Fig. 1e, 1f) indicating ongoing neuroinflammation and demyelination as demonstrated earlier for this model [2]. At week 3 no substantial genotype difference was obvious. At week 5 of cuprizone treatment, the T_2-weighted signal intensity for TREM2-KO was higher than for TREM2-sol, TREM2-IPD and WT animals (Fig. 1e, 1f). Whereas for WT and TREM2-IPD animals the MRI signal in EC decreased from week 5 to 9 during the recovery phase, for TREM2-sol and TRE2-KO mice it further increased in the same time interval despite discontinuation of cuprizone (Fig. 1f). TREM2-KO displayed an even stronger T_2-weighted MRI signal intensity increase in CC which is quite different to TREM2-sol (Fig. 1f). In TREM2-IPD, TREM2-sol het, TREM2-KO het and WT mice, however, the MRI T2-weighted signal intensity decreased from week 5 to 9 in the combined EC/CC (Fig. S2) but did not return to baseline levels, suggesting only partial spontaneous remyelination as evidenced earlier [2]. In agreement with the T2-weighted signal results, MTR in the EC/CC of WT, homo- and heterozygous TREM2-KO mice at week 5 was significantly lower than at baseline, and while a partial recovery of MTR occurred for WT and heterozygous TREM2-KO animals from week 5 to 9 in the absence of cuprizone, a further reduction happened in homozygous TREM2-KO animals (Fig, 1f, Fig. S3). The behavior of the T_2-weighted signal was also reflected by an increase of the relaxation time T_2 predominantly in the EC of cuprizone-challenged mice and by the sustained T_2 increase in the EC throughout the recovery phase as exemplified for TREM2-sol mice (Fig. S4). Also, MTR reduction consistent with cuprizone-induced demyelination was detected in the CC and EC, but the reduction was more prominent in the EC (Fig. S4). During the recovery phase, MTR in the EC of TREM2-sol mice remained low, while a partial recovery was seen in WT and TREM2-IPD animals (Fig. S4).

Analysis of soluble TREM2 in the brain at the peak of cuprizone intoxication revealed a substantial increase in WT, while TREM2-IPD showed a significant lower level indicating reduced TREM2 shedding (Fig. S5). As expected from BMDM (Fig. S1A), soluble TREM2 levels in TREM2-sol mice were reduced compared to WT and in addition did not show any increase upon cuprizone intoxication (Fig. S5). In the

recovery phase at week 9 soluble TREM2 levels normalized in WT, while in TREM2-IPD no reduction of soluble TREM2 could be observed (Fig. S5).

Cuprizone intoxication for 5 weeks resulted in a robust loss of myelin in the EC and CC of all genotypes as revealed by LFB immunohistochemistry (Fig. 2a), while no obvious genotype-dependent difference in myelin could be observed in animals receiving control food (Fig. S6). In the recovery phase 4 weeks after cuprizone removal weak but similar remyelination in TREM2-IPD and WT mice could be observed, while no remyelination occurred in TREM2-sol and TREM2 KO mice (Fig. 2a). Moreover, cuprizone treatment for 5 weeks reduced the number of oligodendrocytes (GST-π-positive) in CC and EC in all genotypes to the same degree (Fig. 2b), while no obvious genotype-dependent difference in oligodendrocytes could be observed in animals receiving control food (Fig. S4). The GST-π reduction in EC was slightly more pronounced than in CC at 5-week of cuprizone intoxication. In the recovery phase 4 weeks after cuprizone removal TREM2-sol and TREM2-KO mice showed only a slight recovery of GST-π-positive oligodendrocytes in the EC (Fig. 2b). However, in the CC similar recovery rates of oligodendrocytes could be observed for all genotypes except for TREM2-sol mice, which displayed even enhanced GST-π numbers than TREM2-sol mice on control food (Fig. 2b). Thus, in the absence of TREM2 oligodendrocytes were able to recover in CC to nearly normal levels while in TREM2-sol mice oligodendrocyte recovery was exceeding controls. However, the recovered oligodendrocytes in the CC in TREM2-KO mice were unable to exert their myelination function as observed with the absence of Luxol Fast Blue staining (Fig. 2a). The oligodendrocytes in TREM2-sol, nevertheless, were able to remyelinate as indicated by enhanced LFB staining (Fig. 2a).

Staining against dMBP revealed the appearance of myelin debris during intoxication as well as the persistence of myelin debris in the recovery phase in TREM2-sol and TREM2-KO (Fig. 2c). No myelin debris at any time-point was visible in TREM2-IPD and WT mice (Fig. 2c) as well a no myelin debris could be observed in genotype receiving control food (Supp Fig. 6). Interestingly, in CC of TREM2-KO substantial higher levels of myelin debris could be observed than in TREM2-sol (Fig. 2c). In EC the level of dMBP were similar for both TREM2-KO and TREM2-sol at peak of intoxication at week 5, while in the recovery phase dMBP levels reduced in TREM2-sol but not in TREM2-KO (Fig. 2c).

Axonal pathology, characterized by loss of neurite fibers stained with SMI312, could be observed in EC, especially in the recovery phase 4 weeks after cuprizone removal in both TREM2-sol and TREM2-KO mice (Fig. 2d). The axonal pathology and fiber loss seems to be higher in TREM2-KO, as also CC and the cortex showed extensive SMI312 staining reduction (Fig. 2d). This observed axonal pathology was paralleled by increased NF-L levels in plasma (Fig. S7). In contrast, no significant axonal pathology was obvious in TREM2-IPD and WT mice at any time-point (Fig. 2d) as well as no change in plasma NF-L (Fig. S7).

TREM2-IPD as well as TREM2-sol displayed increased and sustained number of microglia and astrocytes which is paralleled in TREM2-sol with an enhancement of both LAMP-1 and TMEM119 in the acute cuprizone model

Microglia in EC and CC increased in numbers and became highly activated after cuprizone intoxication for 5 weeks (Fig. 3a, Fig. S8). In WT mice the expected increase of microglia numbers and activation in EC and CC upon 5-week cuprizone and also a subsequent reduction of both parameters, albeit not to baseline levels, during the 4-week recovery phase on normal food could be observed (Fig. 3a, Fig. S8). An analogous course was observed for GFAP-positive astrocytes in WT animals (Fig. 3d). TREM2-IPD as well as TREM2-sol showed a similar increase in microglia numbers and activation, while TREM2-KO displayed a slightly smaller increase in microglia numbers and reduced microglia activation after the 5-week cuprizone treatment as compared to the other genotypes (Fig. 3a, Fig. S8). Interestingly, in the recovery phase microgliosis in CC further increased for TREM2-IPD, TREM2-sol and TREM2-KO, while in TREM2-sol microglia activation further increased in both EC and CC (Fig. 3a, Fig. S8). A similar effect could be observed for GFAP-positive astrocytes in EC and CC for TREM2-IPD, TREM2-sol and TREM2-KO (Fig. 3d); no reduction of astrocytes during recovery phase, but rather a further increase of astrocytosis especially in CC (Fig. 3d). This observation in TREM2-sol is in stark contrast to some of the cytokines/chemokines measured in the forebrain (Fig. S9). Similarly to TREM2-KO, TREM2-sol only showed a marginal increase or even no substantial increase of MIP-1a, MIP-1b and MCP-1 compared to WT at the peak of cuprizone intoxication. For IP-10 the increase was comparable to WT, but it even further increased in TREM2-sol in the recovery phase (Fig. S9). However, in TREM2-IPD a dramatic increase of all measured cytokines/chemokines could be observed during cuprizone intoxication, while they decreased, but not to baseline levels, during the recovery phase (Fig. S9).

The lysosome-associated membrane protein 1 (LAMP-1) similar to CD68 increases during microglia activation [15] and serves also as an ideal marker for disease-associated microglia [20]. Here, LAMP-1 expression during cuprizone intoxication increased to approximately the same levels in EC of WT, TREM2-IPD and TREM2-sol mice, however, the increase was significantly less pronounced in TREM2-KO mice (Fig. 3b). Interestingly, LAMP-1 staining intensity in EC did not reduce during recovery in TREM2-IPD as was the case in WT mice, again pointing to a persistent microglia activation. In TREM2-sol LAMP-1 staining in EC even further increased during recovery, but the staining pattern was rather diffuse and not punctual anymore (Fig. 3d), indicative of dysfunctional microglia. Similar observations were made for CC as well. TMEM119 is a homeostatic microglia marker which decreases during microglia activation [20]. Here, TMEM119 in EC and CC was already very low in all genotypes in control condition (Fig. S6) and thus no reduction could be observed in WT as well as TREM2-IPD mice (Fig. 3d). However, in TREM2-sol mice TMEM119 expression increased significantly especially in EC and it even further increased during the recovery period (Fig. 3d). This is contrast to TREM2-KO where no such increase of TMEM119 in EC could be observed (Fig. 3d). In CC this increase of TMEM119 was apparent, albeit much less for TREM2-sol, for both genotypes, TREM2-sol and TREM2-KO during recovery phase (Fig. 3d).

Sustained TREM2 activation in TREM2-IPD led to enhanced remyelination in the chronic cuprizone model

TREM2-IPD and WT mice were characterized in the chronic 12-week cuprizone model with a three-week recovery period (Fig. 4a, 4b). For both strains of animals, MRI revealed significantly enhanced T_2-weighted signal in EC and CC during the course of cuprizone intoxication and the recovery period (Fig. 4c), consistent with demyelination/neuroinflammation [2]. However, the signal increase in EC was significantly lower for TREM2-IPD mice, whereas in CC there was a non-significant trend for this effect (Fig. 4c). Moreover, significantly increased relaxation time T_2 values and significantly reduced MTR were detected in both EC and CC in this chronic model, although no significant differences in these parameters were found for WT and TREM2-IPD mice (Fig. S10). The in vivo observations were consistent with LFB staining at week 15 showing an increase of myelination especially in EC in TREM2-IPD compared to WT (Fig. 4d). Similarly, an increased number of GST-π-positive oligodendrocytes in EC could be observed after 3-week recovery in TREM2-IPD compared to WT (Fig. 4e). Microglia, astrocytes and LAMP-1 staining were similarly increased in the chronic cuprizone model in the recovery phase (Fig. S11) as already observed in the acute model (Fig. 3). This indicates that in harsher more chronic pathological conditions sustained TREM2 activation in TREM2-IPD mice leads to beneficial effects on myelination processes.

Discussion

TREM2 is essential for microglia to respond appropriately in certain disease conditions as well as to fulfill homeostatic functions during development and aging. Human genetics revealed several mutations in TREM2 leading to a loss-of-function and to a disease called Nasu-Hakola which displays among others excessive central myelination defects [6]. Similarly, mice completely lacking TREM2 showed a dramatic impairment in microglia responses and myelination processes in the cuprizone model as previously described [3, 5, 35, 37]. Here, we confirm these findings in TREM2-KO mice in the 5-week cuprizone model by additionally applying non-invasive longitudinal MRI measurements and different quantitative histological assessments. Furthermore, we report for the first time that mice expressing soluble-only TREM2 show similar pathologies as TREM2-KO, but, nevertheless, also display explicit differences in microglia activation. Finally, sustained TREM2 activation in TREM2-IPD show enhanced remyelination and persistent microglia activation.

MRI provided the opportunity to analyze non-invasively demyelination/remyelination processes in several brain areas. We had demonstrated earlier the significant correlation/negative correlation between T_2-weighted signal intensity/MTR and histological parameters of myelin content in the cuprizone model [2]. In other words, reduced myelin content would be reflected in a reduced MTR respectively in an increased signal intensity. Consistent with the validation work performed earlier [2], upon acute cuprizone administration there was a significant T_2-weighted signal increase and MTR reduction in EC and CC for all genotypes. When cuprizone was discontinued at week 5, there was a partial reduction of T_2-weighted signal/increase of MTR for WT, TREM2-IPD and heterozygous TREM2-sol as well as heterozygous TREM2-KO mice, in agreement with partial remyelination at week 9 evidenced histologically. Exceptions were homozygous TREM2-sol and TREM2-KO animals, for which the signal intensity further increased and MTR further reduced despite cuprizone discontinuation. Based on previous studies in the same

model [2] and histological analysis carried out here, the higher MRI signal intensity for TREM2-sol and TREM2-KO mice might be related to debris accumulation and progression of neuroinflammation despite the interruption of the cuprizone treatment. Of note, at week 5 of cuprizone administration, homozygous TREM2-KO mice displayed a lower level of MTR reduction, whereas there was a higher signal intensity in these animals compared to the other genotypes. Analogous results were obtained for EC of TREM2-sol mice. Histology revealed the appearance of myelin debris during intoxication as well as the persistence of debris in the recovery phase in EC and CC of TREM2-KO and particularly in EC of TREM2-sol mice. The discrepancy between MRI signal and MTR at week 5 for these animals might be linked to poor myelin debris removal, stressing the importance of assessing both parameters. This had already been pointed out earlier for prophylactic treatment of WT mice with the colony stimulating factor 1 receptor (CSF1R) kinase inhibitor, BLZ945, in the same cuprizone model [2]: differences between MRI signal intensity and MTR changes could be explained by the accumulation of debris in EC. These observations are consistent as well with the fact that oligogendrocyte ablation was reported to result only in minor MTR decrease due to inefficient removal of myelin debris [34]. During chronic cuprizone dosing for 12 weeks, T_2-weighted signal in EC and CC was increased with respect to baseline values but significantly lower in EC of TREM2-IPD compared to WT mice. Histology at week 15 demonstrated a higher myelin content in EC of TREM2-IPD mice. MTR was reduced in both EC and CC with respect to baseline throughout the experiment, but it did not display significant differences between TREM2-IPD and WT animals despite being larger for TREM2-IPD at all-time points measured. This suggests a lower sensitivity of MTR compared to T_2-weighted signal analyses to follow pathology in this model.

There is strong evidence that microglia are vital for normal myelinogenesis, for clearance of myelin debris and modulation of oligodendrocyte precursor cell (OPC) differentiation [11, 12, 14, 22, 40, 45]. The inefficient clearance of myelin debris is, amongst other factors, responsible for an inefficient remyelination [3, 5, 35, 37]. During the recovery phase following chronic cuprizone dosing sustained microglia activation via cleavage-reduced TREM2 resulted in enhanced remyelination in EC in TREM2-IPD mice. Analogously, enhanced microglia activation in TREM2-IPD, as observed by increased microglia numbers and activation as well as brain cytokines/chemokines, led to similar remyelination levels as in WT during the recovery after 5 weeks of cuprizone intoxication. This could be explained by the endogenous repair mechanisms that are able to respond in this acute model quite readily [12, 21]. Furthermore, astrocytes are also highly activated in TREM2-IPD and the astrocyte levels stay high during the recovery that also could contribute to an augmented remyelination process [38, 43].

In the acute cuprizone model, similar pathology was observed in EC of TREM2-sol mice expressing only the soluble form of TREM2 and in mice completely lacking TREM2; reymelination was impaired and thus axonal pathology was apparent. TREM2-sol as well as TREM-KO displayed massive appearance of myelin debris in EC, which hampered proper remyelination processes [29, 30]. Interestingly, in TREM2-sol mice microglia were quite readily induced by cuprizone, translated into increased numbers and activation, and also LAMP-1 (lysosomal-associated membrane protein 1) levels were comparable to those observed in EC of WT and TREM2-IPD animals during cuprizone intoxication. However, the microglia from TREM2-

sol mice were not capable of removing myelin debris. LAMP-1, a marker for phagolysosomes, are enriched in highly phagocytic microglia [28, 31] as well as in astrocytes [38]. Astrocytes, which were highly induced in the EC of TREM2-sol and TREM2-KO mice, have been hypothesized to cause detrimental effects on myelination, depending on the pathology context [38]. It also has been shown that astrocytes crosstalk to microglia and support proper microglia function [12, 36, 43]. However, in the present study microglia in TREM2-sol and TREM2-KO seemed to be dysfunctional and could not properly respond to the insult as indicated by the lack of cytokine and chemokine induction as well as by the increase of expression of the homeostatic marker TMEM119 [3, 20, 31]. Finally, LAMP-1 induction was further increased in the recovery phase in TREM2-sol in stark contrast to TREM2-KO, but punctate staining was lost and a rather diffuse LAMP-1 appearance was observed. This could indicate a loss of proper LAMP-1 localization in microglia/astrocytes and thus lead to lysosomal dysfunction, but might also be indicative of neuronal pathology as observed in other neurological diseases [23, 57]. Although less pronounced axonal loss was observed in TREM2-sol compared to TREM2-KO mice, the increase in LAMP-1 could indicate more neuronal stress, which was also suggested by an increase in NF-L in plasma. Nevertheless, the persistent microglia activation with the increased LAMP-1 induction paralleled by massive increase of TMEM119 in TREM2-sol shows that soluble TREM2 seems to be involved in regulating, albeit improperly, microglia. Similarly, it has been shown that soluble TREM2 is enhancing microglial inflammatory responses [54]. However, in contrast to our results it has been reported that soluble TREM2 protects against amyloid-beta-driven pathology in an AD model [55]. This difference to the cuprizone model could be explained by the use of a more chronic model as it is the case for AD and the expression of higher amounts of soluble TREM2 via AAV. Of note, the observed reduced levels of soluble TREM2 in TREM2-sol mice might not be sufficient to induce positive outcomes. Furthermore, in CSF of humans an enhanced level of soluble TREM2 seems to correlate with an attenuated clinical progression in AD [9]. Finally, the choice of the model used is also important to decipher the directionality of TREM2-dependent effects [24]. The beneficial effect of cleavage-reduced TREM2 in TREM2-IPD mice was observed in the chronic cuprizone model. In contrast, enhanced pathology of cleavage-reduced TREM2 was observed in an AD model [7]. Further studies are needed to decipher these TREM2-dependent cellular processes in different preclinical models.

Regional differences of remyelination and neuroinflammation could be observed in the acute cuprizone model. While microglia numbers decreased during recovery in EC of TREM2-IPD, they rather increased in CC of the same animals. This was similar to TREM2-KO, however in TREM2-sol mice microglia increase was observed in both regions, EC and CC. Interestingly, a similar brain region-specific finding on microglia was observed when mice were prophylactically treated with the CSF1R kinase inhibitor, BLZ945, in the acute cuprizone model [2]. While microglia were depleted in CC by BLZ945, microglia specifically in EC were insensitive and still remained. Of note, an interaction of TREM2 and CSF1R has been recently hypothesized [4] indicating a conveyance of both pathways leading to similar changes. Furthermore, it is now well-established that regional heterogeneity of microglia exists, e.g. on transcriptional profile, functionality and number [1, 31, 33, 56]. Furthermore, there seems to be a direct correlation between the amount of myelin debris and the improper microglia activation in EC of TREM2-sol mice. This in turn

leads to a lack of remyelination or even to further demyelination despite some recovery of oligodendrocytes, as the latter are not capable of remyelinating. Of note, the amount of myelin debris in CC of TREM2-sol mice was significantly smaller than that quantified in EC. Given the fact that improper microglia activation was seen in both brain areas, it seems reasonable to conclude that the oligodendrocytes' recovery and ability to remyelinate in CC of TREM2-sol animals was due to the smaller amount of debris in this region compared to EC. In contrast, in TREM2-KO oligodendrocytes were not capable of promoting remyelination in CC during the recovery phase, although improper microglia activation was similar to that in TREM2-sol. It has been shown that brain-region specific non-myelinating oligodendrocyte recovery can occur despite massive presence of myelin debris [17, 52] and this again calls for careful analysis of regional differences and regional cell population heterogeneities.

In summary, our results further strengthen the role of TREM2 in proper microglia function towards brain insults, in particular myelin damage, and show for the first time that sustained TREM2 activation enhances remyelination and soluble TREM2 induces myelin clearance defects and a lack of remyelination. These results put TREM2 in the spotlight as an interesting target to modulate microglia and myelination processes in different myelination diseases.

Abbreviations

cc
corpus callosum
ec
external capsule
GFAP
glial fibrillary acidic protein
GST-π
glutathione S-transferase-π
KO
knockout
LFB
luxol fast blue
MBP
myelin basic protein
dMBP
debris of MBP
MRI
magnetic resonance imaging
ms
millisecond
MTR
magnetization transfer ratio

OD
optical density
OPC
oligodendrocyte precursor cell
SD
standard deviation
SEM
standard error of the mean
TREM2
Triggering receptor expressed on myeloid cells 2
WT
wildtype

Declarations

Animal studies described in this report were approved by the Swiss Cantonal Veterinary Authority of Basel City, Switzerland, under the license number BS-2711.

Availability of data and materials

All data generated or analyzed during this study are included in this published article

Competing interest

All authors are or have been employees and shareholders of Novartis Pharma AG, Basel Switzerland.

Funding

This work was funded by Novartis Pharma AG.

Author contributions

NB, DS, DF, FG, UN designed research. AN, SZ, SJ, TS, RB, DF, AD, SR, NB, DS performed research. NB, AD, SZ, RB, SJ, TS, DF, WF, DS analyzed data. NB, DS wrote the paper. All authors read and approved the final manuscript

Acknowledgment

We thank Hong Lei, Thomas Nicholson, Daniel Breustedt, Wibke Schwarzer for the generation and genotyping of transgenic mice. We thank Irena Brzak for technical assistance.

Consent for publication

Consent for publication is granted from Novartis Institutes for BioMedical Research.

References

1. Amor S, Mcnamara NB, Gerrits E, Manuel ·, Marzin C, Kooistra SM, Miron VE, Nutma E. White matter microglia heterogeneity in the CNS. Acta Neuropathol 2021. 2021;1:1–17. doi:10.1007/s00401-021-02389-x.
2. Beckmann N, Giorgetti E, Neuhaus A, Zurbruegg S, Accart N, Smith P, Perdoux J, Perrot L, Nash M, Desrayaud S, Wipfli P, Frieauff W, Shimshek DR. Brain region-specific enhancement of remyelination and prevention of demyelination by the CSF1R kinase inhibitor BLZ945. Acta Neuropathol Commun. 2018;6:9. doi:10.1186/s40478-018-0510-8.
3. Cantoni C, Bollman B, Licastro D, Xie M, Mikesell R, Schmidt R, Yuede CM, Galimberti D, Olivecrona G, Klein RS, Cross AH, Otero K, Piccio L. TREM2 regulates microglial cell activation in response to demyelination in vivo. Acta Neuropathol. 2015. doi:10.1007/s00401-015-1388-1.
4. Cheng B, Li X, Dai K, Duan S, Rong Z, Chen Y, Lü L, Liu Z, Huang X, Xu H, Zhang YW, Zheng H. Triggering Receptor Expressed on Myeloid Cells-2 (TREM2) Interacts With Colony-Stimulating Factor 1 Receptor (CSF1R) but Is Not Necessary for CSF1/CSF1R-Mediated Microglial Survival. Front Immunol. 2021;12:1–13. doi:10.3389/fimmu.2021.633796.
5. Cignarella F, Filipello F, Bollman B, Cantoni C, Locca A, Mikesell R, Manis M, Ibrahim A, Deng L, Benitez BA, Cruchaga C, Licastro D, Mihindukulasuriya K, Harari O, Buckland M, Holtzman DM, Rosenthal A, Schwabe T, Tassi I, Piccio L. TREM2 activation on microglia promotes myelin debris clearance and remyelination in a model of multiple sclerosis. Acta Neuropathol. 2020. doi:10.1007/s00401-020-02193-z.
6. Dardiotis E, Siokas V, Pantazi E, Dardioti M, Rikos D, Xiromerisiou G, Markou A, Papadimitriou D, Speletas M, Hadjigeorgiou GM. A novel mutation in TREM2 gene causing Nasu-Hakola disease and review of the literature. Neurobiol Aging. 2017;53:194.e13.
-194.e22
. doi: 10.1016/j.neurobiolaging.2017.01.015.
7. Dhandapani R, Neri M, Bernhard M, Brzak I, Schweizer T, Rudin S, Joller S, Berth R, Waldt A, Cuttat R, Naumann U, Keller CG, Roma G, Feuerbach D, Shimshek DR, Neumann U, Gasparini F, Galimberti I. (2021) Sustained TREM2 stabilization accelerates microglia heterogeneity and Aβ pathology in a mouse model of Alzheimer's disease. bioRxiv 2021.06.23.449405.
8. Dong Y, D'Mello C, Pinsky W, Lozinski BM, Kaushik DK, Ghorbani S, Moezzi D, Brown D, Melo FC, Zandee S, Vo T, Prat A, Whitehead SN, Yong VW. Oxidized phosphatidylcholines found in multiple sclerosis lesions mediate neurodegeneration and are neutralized by microglia. Nat Neurosci. 2021. doi:10.1038/s41593-021-00801-z.
9. Ewers M, Franzmeier N, Suárez-Calvet M, Morenas-Rodriguez E, Caballero MAA, Kleinberger G, Piccio L, Cruchaga C, Deming Y, Dichgans M, Trojanowski JQ, Shaw LM, Weiner MW, Haass C, Alzheimer's Disease Neuroimaging Initiative. Increased soluble TREM2 in cerebrospinal fluid is associated with reduced cognitive and clinical decline in Alzheimer's disease. Sci Transl Med 11. 2019. doi:10.1126/scitranslmed.aav6221.

10. Feuerbach D, Schindler P, Barske C, Joller S, Beng-Louka E, Worringer KA, Kommineni S, Kaykas A, Ho DJ, Ye C, Welzenbach K, Elain G, Klein L, Brzak I, Mir AK, Farady CJ, Aichholz R, Popp S, George N, Neumann U. ADAM17 is the main sheddase for the generation of human triggering receptor expressed in myeloid cells (hTREM2) ectodomain and cleaves TREM2 after Histidine 157. Neurosci Lett. 2017;660:109–14. doi:10.1016/j.neulet.2017.09.034.
11. Gouna G, Klose C, Bosch-Queralt M, Liu L, Gokce O, Schifferer M, Cantuti-Castelvetri L, Simons M. (2021) TREM2-dependent lipid droplet biogenesis in phagocytes is required for remyelination. J Exp Med 218. doi:10.1084/jem.20210227.
12. Gudi V, Gingele S, Skripuletz T, Stangel M. Glial response during cuprizone-induced de- and remyelination in the CNS: lessons learned. Front Cell Neurosci. 2014;8:73. doi:10.3389/fncel.2014.00073.
13. Haase A, Matthaei D, Hänicke W, Frahm J. Dynamic digital subtraction imaging using fast low-angle shot MR movie sequence. Radiology. 1986;160:537–41. doi:10.1148/radiology.160.2.3523597.
14. Hagemeyer N, Hanft K-M, Akriditou M-A, Unger N, Park ES, Stanley ER, Staszewski O, Dimou L, Prinz M. Microglia contribute to normal myelinogenesis and to oligodendrocyte progenitor maintenance during adulthood. Acta Neuropathol. 2017. doi:10.1007/s00401-017-1747-1.
15. Hammond TR, Dufort C, Dissing-Olesen L, Giera S, Young A, Wysoker A, Walker AJ, Gergits F, Segel M, Nemesh J, Marsh SE, Saunders A, Macosko E, Ginhoux F, Chen J, Franklin RJM, Piao X, McCarroll SA, Stevens B. Single-Cell RNA Sequencing of Microglia throughout the Mouse Lifespan and in the Injured Brain Reveals Complex Cell-State Changes. Immunity. 2019;50:253–71.e6. doi:10.1016/j.immuni.2018.11.004.
16. Hennig J, Nauerth A, Friedburg H. RARE imaging: A fast imaging method for clinical MR. Magn Reson Med. 1986;3:823–33. doi:10.1002/mrm.1910030602.
17. Jäkel S, Agirre E, Falcão AM, Bruggen D van, Lee KW, Knuesel I, Malhotra D, ffrench-Constant C, Williams A, Castelo-Branco G. Altered human oligodendrocyte heterogeneity in multiple sclerosis. Nat 2019. 2019;2:1. doi:10.1038/s41586-019-0903-2.
18. Jay TR, Miller CM, Cheng PJ, Graham LC, Bemiller S, Broihier ML, Xu G, Margevicius D, Karlo JC, Sousa GL, Cotleur AC, Butovsky O, Bekris L, Staugaitis SM, Leverenz JB, Pimplikar SW, Landreth GE, Howell GR, Ransohoff RM, Lamb BT. TREM2 deficiency eliminates TREM2 + inflammatory macrophages and ameliorates pathology in Alzheimer's disease mouse models. J Exp Med. 2015;212:287–95. doi:10.1084/jem.20142322.
19. Jay TR, von Saucken VE, Landreth GE. TREM2 in Neurodegenerative Diseases. Mol Neurodegener. 2017;12:56. doi:10.1186/s13024-017-0197-5.
20. Keren-Shaul H, Spinrad A, Weiner A, Matcovitch-Natan O, Dvir-Szternfeld R, Ulland TK, David E, Baruch K, Lara-Astaiso D, Toth B, Itzkovitz S, Colonna M, Schwartz M, Amit I. A Unique Microglia Type Associated with Restricting Development of Alzheimer's Disease. Cell. 2017;169:1276–90.e17. doi:10.1016/j.cell.2017.05.018.

21. Kipp M, Clarner T, Dang J, Copray S, Beyer C. The cuprizone animal model: new insights into an old story. Acta Neuropathol. 2009;118:723–36. doi:10.1007/s00401-009-0591-3.
22. Lampron A, Larochelle A, Laflamme N, Préfontaine P, Plante M-M, Sánchez MG, Yong VW, Stys PK, Tremblay M-È, Rivest S. Inefficient clearance of myelin debris by microglia impairs remyelinating processes. J Exp Med. 2015;212:481–95. doi:10.1084/jem.20141656.
23. Lee S-H, Meilandt WJ, Xie L, Gandham VD, Ngu H, Barck KH, Rezzonico MG, Imperio J, Lalehzadeh G, Huntley MA, Stark KL, Foreman O, Carano RAD, Friedman BA, Sheng M, Easton A, Bohlen CJ, Hansen DV. Trem2 restrains the enhancement of tau accumulation and neurodegeneration by β-amyloid pathology. Neuron. 2021;109:1283–301.e6. doi:10.1016/j.neuron.2021.02.010.
24. Lee S, Meilandt WJ, Xie L, Gandham VD, Ngu H, Barck KH, Rezzonico MG, Imperio J, Lalehzadeh G, Huntley MA, Stark KL, Foreman O, Carano RAD, Friedman BA, Sheng M, Easton A, Bohlen CJ, Hansen DV. Trem2 restrains the enhancement of tau accumulation and neurodegeneration by β-amyloid pathology. Neuron. 2021;109:1283–301.e6. doi:10.1016/j.neuron.2021.02.010.
25. Li H. A statistical framework for SNP calling, mutation discovery, association mapping and population genetical parameter estimation from sequencing data. Bioinformatics. 2011;27:2987–93. doi:10.1093/bioinformatics/btr509.
26. Li H, Durbin R. Fast and accurate long-read alignment with Burrows-Wheeler transform. Bioinformatics. 2010;26:589–95. doi:10.1093/bioinformatics/btp698.
27. Li H, Handsaker B, Wysoker A, Fennell T, Ruan J, Homer N, Marth G, Abecasis G, Durbin R. The Sequence Alignment/Map format and SAMtools. Bioinformatics. 2009;25:2078–9. doi:10.1093/bioinformatics/btp352.
28. Liu Z, Condello C, Schain A, Harb R, Grutzendler J. CX3CR1 in microglia regulates brain amyloid deposition through selective protofibrillar amyloid-β phagocytosis. J Neurosci. 2010;30:17091–101. doi:10.1523/JNEUROSCI.4403-10.2010.
29. Lloyd AF, Davies CL, Holloway RK, Labrak Y, Ireland G, Carradori D, Dillenburg A, Borger E, Soong D, Richardson JC, Kuhlmann T, Williams A, Pollard JW, des Rieux A, Priller J, Miron VE. Central nervous system regeneration is driven by microglia necroptosis and repopulation. Nat Neurosci. 2019;22:1046–52. doi:10.1038/s41593-019-0418-z.
30. Lloyd AF, Miron VE. (2019) The pro-remyelination properties of microglia in the central nervous system. Nat Rev Neurol 29–34. doi:10.1038/s41582-019-0184-2.
31. Masuda T, Sankowski R, Staszewski O, Prinz M. Microglia Heterogeneity in the Single-Cell Era. Cell Rep. 2020;30:1271–81. doi:10.1016/j.celrep.2020.01.010.
32. McQuade A, Kang YJ, Hasselmann J, Jairaman A, Sotelo A, Coburn M, Shabestari SK, Chadarevian JP, Fote G, Tu CH, Danhash E, Silva J, Martinez E, Cotman C, Prieto GA, Thompson LM, Steffan JS, Smith I, Davtyan H, Cahalan M, Cho H, Blurton-Jones M. Gene expression and functional deficits underlie TREM2-knockout microglia responses in human models of Alzheimer's disease. Nat Commun. 2020;11:5370. doi:10.1038/s41467-020-19227-5.

33. Monier A, Evrard P, Gressens P, Verney C. Distribution and differentiation of microglia in the human encephalon during the first two trimesters of gestation. J Comp Neurol. 2006;499:565–82. doi:10.1002/cne.21123.
34. Mueggler T, Pohl H, Baltes C, Riethmacher D, Suter U, Rudin M. MRI signature in a novel mouse model of genetically induced adult oligodendrocyte cell death. NeuroImage. 2012;59:1028–36. doi:10.1016/j.neuroimage.2011.09.001.
35. Nugent AA, Lin K, Van Lengerich B, Lianoglou S, Przybyla L, Davis SS, Llapashtica C, Wang J, Kim DJ, Xia D, Lucas A, Baskaran S, Haddick PCG, Lenser M, Earr TK, Shi J, Dugas JC, Andreone BJ, Logan T, Solanoy HO, Chen H, Srivastava A, Poda SB, Sanchez PE, Watts RJ, Sandmann T, Astarita G, Lewcock JW, Monroe KM, Di Paolo G. (2019) TREM2 Regulates Microglial Cholesterol Metabolism Upon Chronic Phagocytic Challenge. SSRN Electron J 1–18. doi:10.2139/ssrn.3444596.
36. Petković F, Campbell IL, Gonzalez B, Castellano B. Astrocyte-targeted production of interleukin-6 reduces astroglial and microglial activation in the cuprizone demyelination model: Implications for myelin clearance and oligodendrocyte maturation. Glia. 2016. doi:10.1002/glia.23043.
37. Poliani PL, Wang Y, Fontana E, Robinette ML, Yamanishi Y, Gilfillan S, Colonna M. TREM2 sustains microglial expansion during aging and response to demyelination. J Clin Invest. 2015;125:2161–70. doi:10.1172/JCI77983.
38. Ponath G, Ramanan S, Mubarak M, Housley W, Lee S, Sahinkaya FR, Vortmeyer A, Raine CS, Pitt D. Myelin phagocytosis by astrocytes after myelin damage promotes lesion pathology. Brain. 2017;140:399–413. doi:10.1093/brain/aww298.
39. Rangaraju S, Dammer EB, Raza SA, Rathakrishnan P, Xiao H, Gao T, Duong DM, Pennington MW, Lah JJ, Seyfried NT, Levey AI. Identification and therapeutic modulation of a pro-inflammatory subset of disease-associated-microglia in Alzheimer's disease. Mol Neurodegener. 2018;13:24. doi:10.1186/s13024-018-0254-8.
40. Safaiyan S, Besson-Girard S, Kaya T, Cantuti-Castelvetri L, Liu L, Ji H, Schifferer M, Gouna G, Usifo F, Kannaiyan N, Fitzner D, Xiang X, Rossner MJ, Brendel M, Gokce O, Simons M. White matter aging drives microglial diversity. Neuron. 2021;109:1100–17.e10. doi:10.1016/j.neuron.2021.01.027.
41. Santos EN, Fields RD. Regulation of myelination by microglia. Sci Adv. 2021;7:573–85. doi:10.1126/sciadv.abk1131.
42. Schlepckow K, Monroe KM, Kleinberger G, Cantuti-Castelvetri L, Parhizkar S, Xia D, Willem M, Werner G, Pettkus N, Brunner B, Sülzen A, Nuscher B, Hampel H, Xiang X, Feederle R, Tahirovic S, Park JI, Prorok R, Mahon C, Liang C, Shi J, Kim DJ, Sabelström H, Huang F, Di Paolo G, Simons M, Lewcock JW, Haass C. Enhancing protective microglial activities with a dual function TREM 2 antibody to the stalk region. EMBO Mol Med. 2020. doi:10.15252/emmm.201911227.
43. Skripuletz T, Hackstette D, Bauer K, Gudi V, Pul R, Voss E, Berger K, Kipp M, Baumgärtner W, Stangel M. Astrocytes regulate myelin clearance through recruitment of microglia during cuprizone-induced demyelination. Brain. 2013;136:147–67. doi:10.1093/brain/aws262.

44. Tagge I, O'Connor A, Chaudhary P, Pollaro J, Berlow Y, Chalupsky M, Bourdette D, Woltjer R, Johnson M, Rooney W. Spatio-temporal patterns of demyelination and remyelination in the cuprizone mouse model. PLoS ONE. 2016;11:1–24. doi:10.1371/journal.pone.0152480.
45. Taylor DL, Pirianov G, Holland S, McGinnity CJ, Norman AL, Reali C, Diemel LT, Gveric D, Yeung D, Mehmet H. Attenuation of proliferation in oligodendrocyte precursor cells by activated microglia. J Neurosci Res. 2010;88:1632–44. doi:10.1002/jnr.22335.
46. Torkildsen O, Brunborg LA, Myhr K-M, Bø L. The cuprizone model for demyelination. Acta Neurol Scand Suppl. 2008;188:72–6. doi:10.1111/j.1600-0404.2008.01036.x.
47. Ulland TK, Song WM, Huang SCC, Ulrich JD, Sergushichev A, Beatty WL, Loboda AA, Zhou Y, Cairns NJ, Kambal A, Loginicheva E, Gilfillan S, Cella M, Virgin HW, Unanue ER, Wang Y, Artyomov MN, Holtzman DM, Colonna M. TREM2 Maintains Microglial Metabolic Fitness in Alzheimer's Disease. Cell. 2017;170:649–63.e13. doi:10.1016/j.cell.2017.07.023.
48. De Vree PJP, De Wit E, Yilmaz M, Van De Heijning M, Klous P, Verstegen MJAM, Wan Y, Teunissen H, Krijger PHL, Geeven G, Eijk PP, Sie D, Ylstra B, Hulsman LOM, Van Dooren MF, Van Zutven LJCM, Van Den Ouweland A, Verbeek S, Van Dijk KW, Cornelissen M, Das AT, Berkhout B, Sikkema-Raddatz B, Van Den Berg E, Van Der Vlies P, Weening D, Den Dunnen JT, Matusiak M, Lamkanfi M, Ligtenberg MJL, Ter Brugge P, Jonkers J, Foekens JA, Martens JW, Van Der Luijt R, Van Amstel HKP, Van Min M, Splinter E, De Laat W. Targeted sequencing by proximity ligation for comprehensive variant detection and local haplotyping. Nat Biotechnol. 2014;32:1019–25. doi:10.1038/nbt.2959.
49. Wang S, Mustafa M, Yuede CM, Salazar SV, Kong P, Long H, Ward M, Siddiqui O, Paul R, Gilfillan S, Ibrahim A, Rhinn H, Tassi I, Rosenthal A, Schwabe T, Colonna M. (2020) Anti-human TREM2 induces microglia proliferation and reduces pathology in an Alzheimer's disease model. J Exp Med 217. doi:10.1084/jem.20200785.
50. Wang Y, Cella M, Cirrito JR, Colonna M, Wang Y, Cella M, Mallinson K, Ulrich JD, Young KL, Robinette ML. (2015) TREM2 Lipid Sensing Sustains the Microglial Response in an Alzheimer ' s Disease Model Article TREM2 Lipid Sensing Sustains the Microglial Response in an Alzheimer ' s Disease Model. Cell 1–11. doi:10.1016/j.cell.2015.01.049.
51. Yaghmoor F. (2014) The Role of TREM2 in Alzheimer's Disease and Other Neurological Disorders. J Alzheimer's Dis Park 04. doi: 10.4172/2161-0460.1000160.
52. Yeung MSY, Djelloul M, Steiner E, Bernard S, Salehpour M, Possnert G, Brundin L, Frisén J. Dynamics of oligodendrocyte generation in multiple sclerosis. Nat doi. 2019. 10.1038/s41586-018-0842-3.
53. Zendedel A, Beyer C, Kipp M. Cuprizone-induced demyelination as a tool to study remyelination and axonal protection. J Mol Neurosci. 2013;51:567–72. doi:10.1007/s12031-013-0026-4.
54. Zhong L, Chen X-F, Wang T, Wang Z, Liao C, Wang Z, Huang R, Wang D, Li X, Wu L, Jia L, Zheng H, Painter M, Atagi Y, Liu C-C, Zhang Y-W, Fryer JD, Xu H, Bu G. (2017) Soluble TREM2 induces inflammatory responses and enhances microglial survival. J Exp Med jem.20160844. doi:10.1084/jem.20160844.

55. Zhong L, Xu Y, Zhuo R, Wang T, Wang K, Huang R, Wang D, Gao Y, Zhu Y, Sheng X, Chen K, Wang N, Zhu L, Can D, Marten Y, Shinohara M, Liu C-C, Du D, Sun H, Wen L, Xu H, Bu G, Chen X-F. Soluble TREM2 ameliorates pathological phenotypes by modulating microglial functions in an Alzheimer's disease model. Nat Commun. 2019;10:1365. doi:10.1038/s41467-019-09118-9.
56. Zia S, Rawji KS, Michaels NJ, Burr M, Kerr BJ, Healy LM, Plemel JR. Microglia Diversity in Health and Multiple Sclerosis. Front Immunol. 2020;11:1–14. doi:10.3389/fimmu.2020.588021.
57. Zigdon H, Meshcheriakova A, Farfel-Becker T, Volpert G, Sabanay H, Futerman AH. Altered lysosome distribution is an early neuropathological event in neurological forms of Gaucher disease. FEBS Lett. 2017;591:774–83. doi:10.1002/1873-3468.12591.

Figures

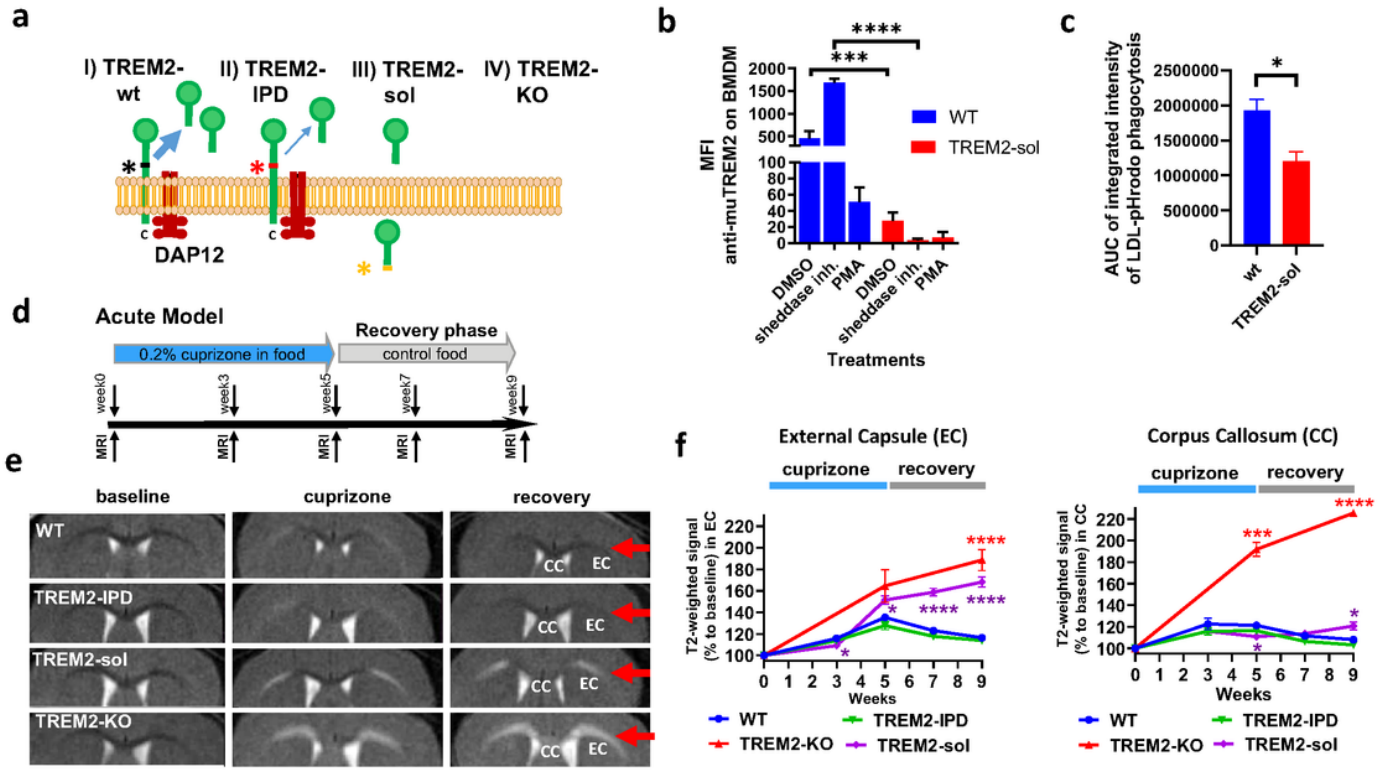

Fig.1

Figure 1

MRI indicated myelination deficits in TREM2-sol and TREM2-KO after 5-week cuprizone and 4-week recovery, while remyelination occurred in TREM2-IPD and WT. **a** Schematic representation of the transgenic TREM2 mice. TREM2-wt (wildtype TREM2), TREM2-IPD (cleavage-reduced TREM2), TREM2-sol (soluble-only TREM2), TREM2-KO (TREM2 knockout). The black, red and yellow asterisks indicate the cleavage site, the mutated cleavage site in TREM2-IPD and the mutated cleavage site in TREM2-sol, respectively. **b** Flow cytometry analysis of murine TREM2 on BMDMs from WT and Trem2-sol mice treated with DMSO, DPC333 (sheddase inhibitor, an ADAM inhibitor) or PMA treatment (n=3 per genotype

and condition). Statistics: Mixed-effects analysis Sidak`s multiple comparison test. ***: p<0.001; ****: p<0.0001. **c** Area-under-the-curve (AUC) analysis of the phagocytosis time-course experiment (see Supp Fig. 1B) in BMDMs from WT and TREM-sol mice with phRodo-Red labeled LDL (low-density lipoprotein). Statistics: Unpaired t-test; *: p<0.05. **d** Schematic diagram of the experimental setup for the cuprizone treatment and recovery. Groups consisted of mice treated for 5 weeks with control food or 0.2% cuprizone in food and then switched back to control food (normal food) for the 4-week recovery. MRI measurements were performed at week 0 (baseline), week 3 and week 5 of cuprizone intoxication, at week 6 (1 week of recovery on control food) and at week 9 (4 weeks of recovery on control food). Mice were culled at week 9 immediately after the last MRI measurement. **e** Representative MRI images acquired from three mice at baseline, at maximal pathology (5 weeks of receiving 0.2% cuprizone) and at recovery (4 weeks after switching to control food) for different genotypes as indicated. **f** Corresponding T2-weighted MRI signal intensity (relative to the signal intensity at baseline) in corpus callosum (CC) and external capsule (EC). Group sizes: n=7 for all genotypes and time-point. Data are shown as means±SEM. Statistics: Anova with random effects comparisons indicated significant differences with respect to WT mice: *0.01<p<0.05, ***0.0001<p<0.001, ****p<0.0001. For each group examined, T2-weighted signals were significantly increased with respect to baseline values (significances not shown).

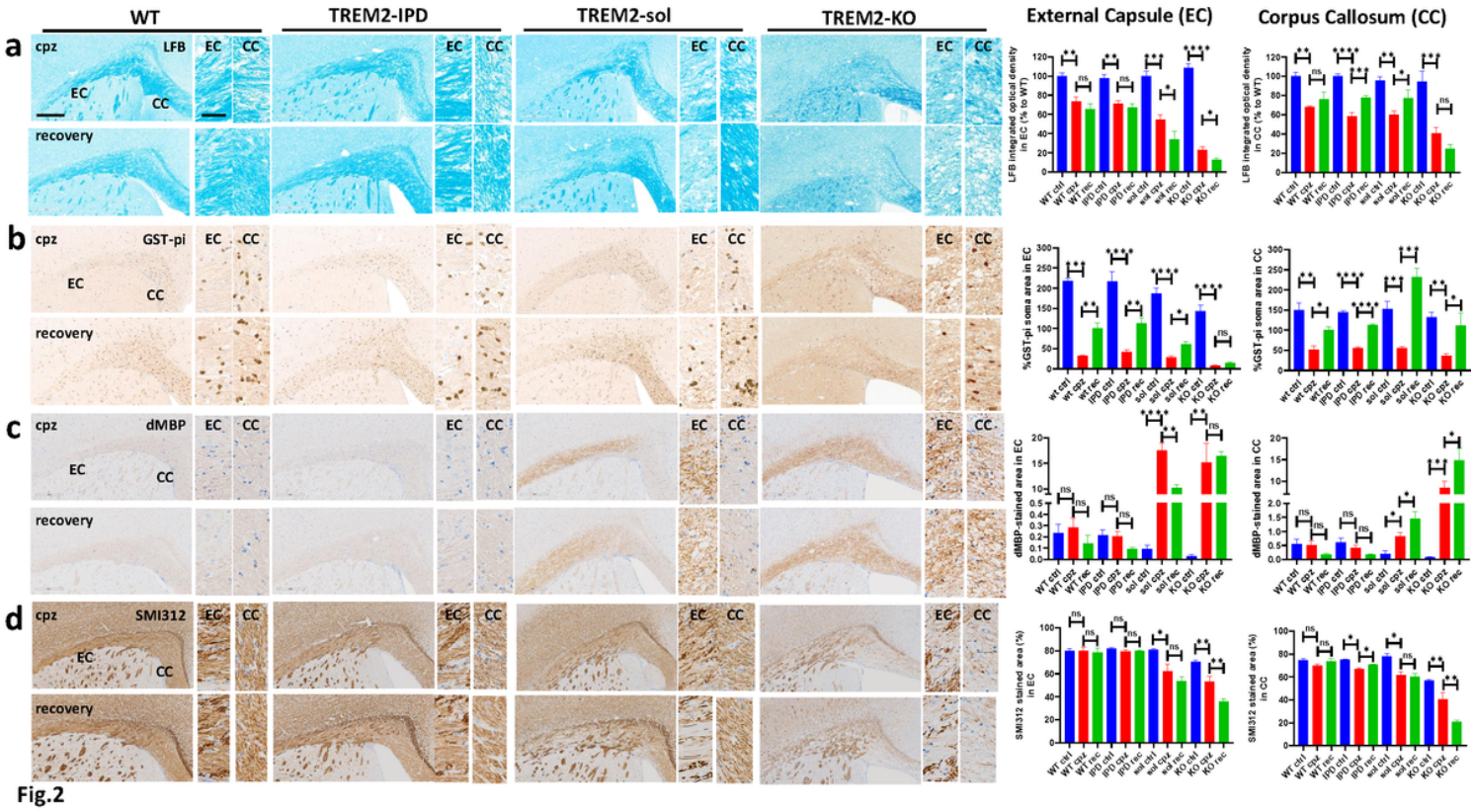

Figure 2

TREM2-IPD and WT mice showed similar myelination processes while in TREM2-sol and TREM2-KO extensive myelin debris, lack of reymelination and axonal pathology was observed. Representative pictures for the different genotypes and time-points from histological stainings detecting **a** Luxol fast blue (LFB) and corresponding quantitative optical density (OD) analysis of LFB in the ec and cc (normalized to WT at control food), **b** detecting mature oligodendrocytes (GST-π) and corresponding image analysis in EC and CC (GST-π soma area in %), **c** myelin basic protein debris (dMBP) for the and corresponding image analysis in EC and CC (dMBP-stained area in %), **d** neurofilament (SMI312) and corresponding image analysis in EC and CC (SMI312-stained area in %). Group sizes: n=7 for all genotypes and time-points. Data shown as means±SEM. WT: wildtype, TREM2-IPD: TREM2 cleavage-reduced, TREM2-sol: TREM2 soluble-only, TREM2-KO: TREM2 knockout. Ctrl: control food, cpz: cuprizone food for 5 weeks, rec: recovery on control food for 4 weeks. EC: external capsul, CC: corpus callosum. Scale bars: 300µm (overview), 50 µm (close-up). Statistics: Holm-Sidak`s multiple comparison test one-way ANOVA (*: 0.01<p<0.05, **: 0.001<p<0.01, ***: 0.0001<p<0.001, ****: p<0.0001, n.s.: not significant).

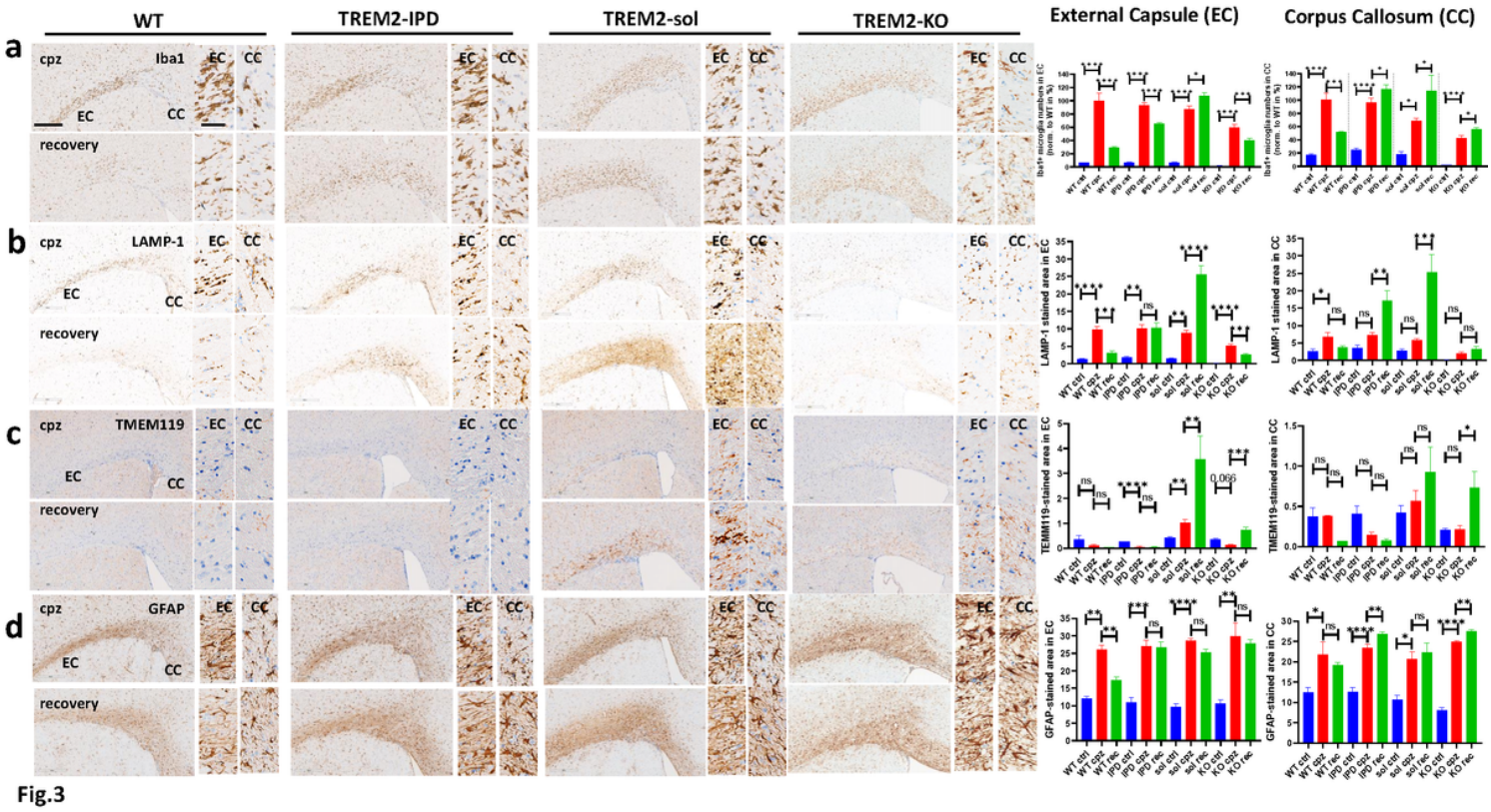

Fig.3

Figure 3

TREM2-IPD as well as TREM2-sol mice showed sustained microglia and astrocyte activation with enhanced LAMP-1 expression while in TREM2-sol also an increase in the homeostatic marker, TMEM119, could be observed. Representative images for the different genotypes and time-points from histological stainings detecting **a** Iba1 and corresponding image analysis of Iba-positive soma numbers in EC and CC (normalized to WT at week 5 cuprizone), **b** LAMP-1 (lysosomal-associated membrane protein 1) and corresponding image analysis in EC and CC (LAMP1-stained area in %), **c** TMEM119 (hoeostatic marker)

and corresponding image analysis in EC and CC (TMEM119-stained area in %), **d** astrocytes (GFAP) and corresponding image analysis in EC and CC (GFAP-stained area in %). Group sizes: n=7 for all genotypes and time-points. Data are shown as means±SEM. WT: wildtype, TREM2-IPD: TREM2 cleavage-reduced, TREM2-sol: TREM2 soluble-only, TREM2-KO: TREM2 knockout. Ctrl: control food, cpz: cuprizone food for 5 weeks, rec: recovery on control food for 4 weeks. EC: external capsul, CC: corpus callosum. Scale bars: 300µm (overview), 50 µm (close-up). Statistics: Holm-Sidak`s multiple comparison test one-way ANOVA (*: 0.01<p<0.05, **: 0.001<p<0.01, ***: 0.0001<p<0.001, ****: p<0.0001, n.s.: not significant).

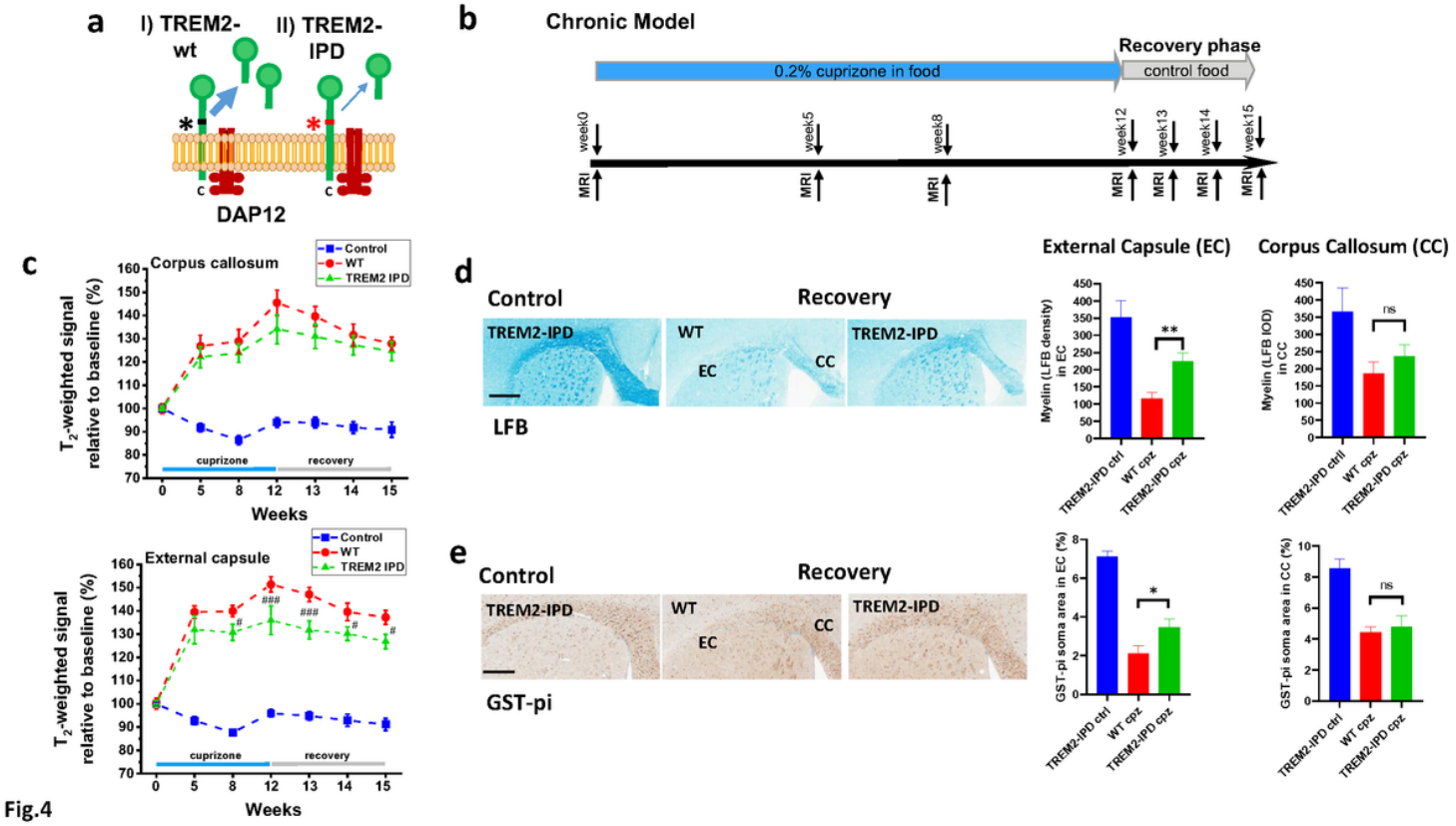

Figure 4

TREM2-IPD showed enhanced myelination in the chronic cuprizone model (12-week cuprizone treatment and 3-week recovery). **a** Schematic representation of the transgenic TREM2 mice. TREM2-wt (wildtype TREM2) and TREM2-IPD (cleavage-reduced TREM2). Black and red asterisks indicate the cleavage site and the mutated cleave site in TREM2-IPD, respectively. **b** Schematic diagram of the experimental setup for the cuprizone treatment and recovery. Groups consisted of mice treated for 12 weeks with control food (normal food) or 0.2% cuprizone in food and then switched back to control food for the 3-week recovery. MRI measurements were performed at time points indicated. Mice were culled at week 15 immediately after the last MRI measurement. **c** T2-weighted signals in cc and ec during the 12-week intoxication period and the recovery phase were significantly increased with respect to baseline values and mice receiving control diet throughout the experiment. The significance levels #0.01<p<0.05 and

###p<0.001 correspond to Anova with random effects comparisons between WT and TREM2-IPD animals. Representative images for the different genotypes and at week 15 from histological stainings detecting **d** Luxol fast blue (LFB) and corresponding quantitative optical density (OD) analysis of LFB in EC and CC, and **e** mature oligodendrocytes (GST-π) and corresponding image analysis in EC and CC (GST-π soma area in %). Group sizes: n=7 for all genotypes and time-points. Data are shown as means±SEM. WT: wildtype, TREM2-IPD: TREM2 cleavage-reduced. Ctrl: control food, rec: recovery on control food for 3 weeks. EC: external capsule, CC: corpus callosum. Scale bars: 500µm. Statistics: T-Test (* 0.01<p<0.05, ** 0.001<p<0.01).

Supplementary Files

This is a list of supplementary files associated with this preprint. Click to download.

- Fig6.png
- Fig7.png
- Fig8.png
- Fig9.png
- Fig10.png
- Fig11.png
- Fig12.png
- Fig13.png
- Fig14.png
- Fig15.png
- Fig16.png